

## NUMERICAL MODELLING OF LANDSLIDE EVENTS USING A COMBINATION OF CONTINUUM AND DISCRETE METHODS

Vincent LEMIALE<sup>1,2\*</sup>, Stuart Mead<sup>1</sup> and Paul CLEARY<sup>1</sup>

<sup>1</sup> CSIRO Mathematics, Informatics and Statistics, Clayton, Victoria 3169, AUSTRALIA

<sup>2</sup> School of geosciences, Monash University, Victoria 3800, AUSTRALIA

\*Corresponding author, E-mail address: Vincent.Lemiale@csiro.au

### ABSTRACT

Landslides are among the most costly natural catastrophes, both in economic and human terms. Most mitigation strategies still rely on a mixture of empirical models and statistical data and so are limited in their ability to quantify the risk in a particular area. However, with the recent advances made in the field of computational mechanics, it has now become possible to develop realistic numerical models of natural disasters. With landslides, a major challenge of the numerical approach is to reliably predict all phases of an event, from its initiation to its propagation including interaction with the surroundings. In this paper, a combination of Smoothed Particle Hydrodynamics (SPH) and Discrete Element Methods (DEM) is considered to address this challenge and to enable the simulation of a complete event. The onset of slope instability is predicted using SPH and a Drucker-Prager yield criterion suitable for pressure dependent materials. The subsequent collapse of the landslide is then simulated by DEM. The failure plane predicted by SPH is used to convert the representation of the mobilised rock or soil mass to a discrete representation. This combined approach is illustrated using an idealised example of slope stability and its potential for simulating complete landslides is demonstrated.

### NOMENCLATURE

$\mathbf{v}$	Velocity
$\mathbf{D}$	Strain rate tensor
$\mathbf{\Omega}$	Spin tensor
$\boldsymbol{\sigma}$	Stress tensor
$\mathbf{S}$	Deviatoric stress tensor
$P$	Pressure
$W$	Kernel function
$l$	smoothing length
$\mathbf{g}$	Gravity vector
$\tau$	Equivalent shear stress $\tau = (0.5 S_{ij} S_{ij})^{1/2}$
$\mathbf{C}^e$	4 <sup>th</sup> order elasticity tensor
$E$	Young's modulus
$\nu$	Poisson's ratio
$G$	Shear modulus
$K$	Bulk modulus
$\rho$	Density
$m$	mass
$c$	Cohesion
$\varphi$	Internal friction angle

$\alpha, k$	Material parameters
$\beta$	Dilatancy angle
$\dot{\lambda}$	Plastic multiplier
$h$	rate of strain hardening for $k$
$t$	Time
$\mathbf{I}$	2 <sup>th</sup> order identity tensor

### INTRODUCTION

Landslides occur in many parts of the world and have a major impact not only on the local population but also in economic terms through the destruction and disruption they cause. They are a threat for two main reasons, namely it is difficult to anticipate when a landslide might occur in a given area and if it does, its consequences are generally difficult to estimate. In most cases, the risk mitigation traditionally relies on risk analysis based on empirical models and statistical data, but these methods are generally not sufficient for a precise quantitative estimate (van Westen et al., 2006). In recent years, models based on deterministic approaches have been proposed to investigate the mechanics of landslides (Hung and McDougall, 2009; van Asch et al., 2007). van Asch et al. (2007) described slope movements as occurring in three phases. The first phase, pre-failure, includes all the deformation that occurs prior to and ultimately determines the triggering factors for large scale slope failure. These triggering factors then initiate the second phase, failure, which leads to the creation of a continuous shear surface or slip plane along which the mass can slide upon. Once the mass is detached along this slip surface, the final post-failure stage occurs. This stage is characterised by significant motion of the landslide mass which is dominated by collisional forces and motion of the granular material. Given the complexity of landslides, a major challenge is to incorporate all phases of an event within one numerical framework.

The pre-failure and failure stages of a landslide are best modelled using continuum soil mechanics approaches because in this phase the slope responds as an equivalent elasto-plastic medium. The post failure stage, however, is a more dynamic process in which the continuum assumption no longer holds and is therefore better predicted using a granular dynamics approach. A combination of continuum and discrete techniques is therefore necessary for a correct representation of the material behaviour. In this paper Smoothed Particle Hydrodynamics (SPH) is combined with the Discrete Element Method (DEM) to simulate a landslide. To predict the onset of instability, a yield criterion suitable for

soils and rocks has been implemented in SPH and is presented in the next section. The failure plane predicted by SPH determines the initial volume of mobilized granular material. The continuum representation of this volume is then converted into a discrete representation for the DEM phase. A combination of factors such as the displacement of the slope, the amount of plastic strain rate and accumulated plastic strain are used as indicators of slope failure for the transition from a continuum to a discrete representation. In this way SPH and DEM can be embedded into one numerical framework to simulate all phases of landslides. The SPH predictions of the onset of slope failure were compared against available data from the literature to validate the model and the results are reported in this paper. Following this validation, the model was used to simulate the subsequent landslide as an illustration of this combined approach.

## NUMERICAL FRAMEWORK

### SPH Formulation for soil mechanics

SPH has been applied to various areas of computational solid mechanics such as fragmentation in solids (Randles and Libersky, 1996), impact of elasto-plastic materials (Cleary, 2010), brittle fracture in rocks (Das and Cleary, 2010) among others. Most of these studies either did not consider plasticity in the constitutive material behaviour or assumed a pressure independent plastic response valid for certain types of materials such as metals. However, a different approach is required in slope stability analysis of soils and rocks because the plastic response of these materials is known to be pressure dependent. Recently, Bui et al. (2008) proposed an SPH formulation suitable for soils and rocks, based on a Drucker-Prager (D-P) yield criterion. In this paper we also consider a D-P criterion to model the plastic behaviour of materials and predict the initiation of a macroscopic instability in a slope.

Conceptually, SPH is a continuum method that can be used to solve partial differential equations for a deforming volume of material discretized using a set of Lagrangian particles. Slope stability requires the solution of both the continuity and momentum equations, which in SPH form may be written respectively as follows (see (Monaghan, 2005) for details):

$$\frac{dp_a}{dt} = \sum_b m_b (\mathbf{v}_a - \mathbf{v}_b) \cdot \nabla_a W_{ab} \quad (1)$$

$$\frac{d\mathbf{v}_a}{dt} = \sum_b m_b \left( \frac{\boldsymbol{\sigma}_a}{\rho_a^2} + \frac{\boldsymbol{\sigma}_b}{\rho_b^2} + \Pi_{ab} \mathbf{I} \right) \cdot \nabla_a W_{ab} + \mathbf{g}_a \quad (2)$$

where  $\Pi_{ab}$  is an artificial viscous stress term as described in (Monaghan, 1992). This includes a Monaghan style tensile instability correction with coefficient 0.3.

These equations must be supplemented with appropriate constitutive laws that are suited to the medium and circumstances under consideration. In standard elasto-plasticity a predictor-corrector scheme is generally used as follows. The material is first assumed to respond elastically and the corresponding elastic stress tensor predicted. If the predicted stress state is found to lie outside the yield surface a plastic correction is required to ensure that the point in the stress space stays on this surface.

In SPH the elastic response of the material is generally assumed hypoelastic and of the form:

$$\boldsymbol{\sigma}^J = 2G\mathbf{D}^e + \left( K - \frac{2G}{3} \right) \text{tr} \mathbf{D}^e \mathbf{I} \quad (3)$$

The Jaumann stress rate  $\boldsymbol{\sigma}^J$  is defined as:

$$\boldsymbol{\sigma}^J = \dot{\boldsymbol{\sigma}} + \boldsymbol{\sigma} \boldsymbol{\Omega} - \boldsymbol{\Omega} \boldsymbol{\sigma} \quad (4)$$

The stress tensor can further be decomposed into its deviatoric and volumetric part:

$$\boldsymbol{\sigma} = \mathbf{S} - P \mathbf{I} \quad (5)$$

where the pressure  $P$  is defined as  $P = -\sigma_{kk}/3$  and is positive in compression.

The first step of the prediction-correction scheme is to assume that the deformation is elastic and to identify  $\mathbf{D}$  with  $\mathbf{D}^e$  in Eq. 3.

Using the stress decomposition of Eq. 5 in Eq. 4 and substituting into Eq. 3 leads to the following elastic prediction:

$$\begin{cases} \dot{\mathbf{S}}^e = 2G\mathbf{D} - \mathbf{S}\boldsymbol{\Omega} + \boldsymbol{\Omega}\mathbf{S} \\ \dot{P}^e = -K \text{tr} \mathbf{D} = -K \nabla \cdot \mathbf{v} \end{cases} \quad (6)$$

To check the validity of the elastic prediction, a D-P yield criterion is considered as follows:

$$\tau - \alpha P - k \begin{cases} < 0 \text{ if elastic} \\ \geq 0 \text{ if yielding} \end{cases} \quad (7)$$

in which  $\alpha$  and  $k$  are material parameters. It is customary to calibrate the D-P criterion so that it approximates the Mohr-Coulomb yield envelope under specific loading conditions. For example, the following calibration is introduced to match both criteria under plane strain conditions:

$$k = \frac{3c}{\sqrt{9 + 12(\tan \varphi)^2}} \quad \alpha = 3 \frac{\tan \varphi}{\sqrt{9 + 12(\tan \varphi)^2}} \quad (8)$$

If the D-P yield criterion is met the material is yielding. Furthermore, if the elastic strains are small compared to the plastic strains, then the following relation holds:

$$\mathbf{D} = \mathbf{D}^e + \mathbf{D}^p \quad (9)$$

Thus the plastic correction can be expressed as:

$$\boldsymbol{\sigma}^J = \mathbf{C}^e : (\mathbf{D} - \mathbf{D}^p) \quad (10)$$

A flow rule is required to estimate the flow due to plastic strain. In soil mechanics the plastic flow is typically represented with a non-associative flow rule:

$$\mathbf{D}^p = \dot{\lambda} \frac{\partial g}{\partial \boldsymbol{\sigma}} \quad (11)$$

The plastic potential  $g$  takes the form:

$$g = \tau - \beta P \quad (12)$$

Using this potential in Eq. 11 leads to:

$$\mathbf{D}^p = \dot{\lambda} \left( \frac{\mathbf{S}}{2\tau} + \frac{\beta}{3} \mathbf{I} \right) \quad (13)$$

which shows that for this model both the deviatoric and volumetric strains are affected by plastic deformation.

Eqs. 6, 10 and 13 can now be combined to derive the final expression for the deviatoric and volumetric components of the stress tensor:

$$\begin{cases} \mathbf{S} = \left( I - \frac{\Delta\lambda G}{\tau^e} \right) \mathbf{S}^e \\ P = P^e + K \beta \Delta\lambda \end{cases} \quad (14)$$

The plastic multiplier  $\Delta\lambda = \dot{\lambda} \Delta t$  is determined by enforcing that the stress state lies on the D-P yield surface. Since linear hardening is assumed for the cohesion, the plastic multiplier can be written in closed form as follows:

$$\Delta\lambda = \frac{\tau^e - \alpha p^e - k}{G + \alpha \beta K + h} \quad (15)$$

The D-P yield surface may be represented by a cone in the stress space with a point of singularity at the apex. At this point, a special procedure is required for the stress correction (de Souza Neto et al., 2008) as the above procedure can lead to unphysical results. In practice, we can detect if a point must be brought back to the apex if the following condition is satisfied:

$$I - \frac{\Delta\lambda G}{\tau^e} \leq 0 \quad (16)$$

This is equivalent to predicting a negative equivalent shear stress  $\tau$ . In this case, the deviatoric stresses are set to 0 and a return to the apex is performed by a pressure correction due to the volumetric strains only.

The slope stability analysis consists of two loading steps. In the first step, the initial stress field due to gravity is determined. To prevent the slope from failing in this phase, a large value of the cohesion is used. The simulation is continued until a mechanical equilibrium is found. Then the cohesion is reset to its physical value in order to analyse the stability of the slope.

As discussed by Bui and Fukagawa (2011), it is necessary in the first loading step to add a damping term to avoid spurious oscillations around equilibrium. To achieve this, the momentum equation (2) was simply modified by adding a damping vector  $\mathbf{D}_a$  written as follows (Bui and Fukagawa, 2011):

$$\mathbf{D}_a^i = -\eta \mathbf{v}_a^i \quad (17)$$

where  $\eta$  is a damping coefficient defined as follows:

$$\eta = \zeta \sqrt{\frac{E}{\rho l^2}}. \quad (18)$$

In this equation  $\zeta$  is a scaling parameter and  $l$  represents the smoothing length used in the SPH discretization.

### Failure detection and slip surface estimation

By using the D-P stress strain model for the slope stability analysis, the pre-failure (stable) and failure stages of landslide events can be effectively represented. In order to predict the landslide run-out, spreading and damage, a transition from the D-P based SPH model to the post-failure granular dynamics model (DEM) is required. For this transition, a method is proposed for detecting the

critical point of failure and, if failure has occurred, the slip surface that has developed.

After loading, the slope deforms (elastically or plastically based on the D-P criterion) due to the internal stresses generated by its weight until it forms either a new stable configuration or a contiguous shear surface in the case of failure. Once the slope has failed or stabilised, its cumulative displacement will become linear, following the standard model for D-P material behaviour. The average acceleration of the entire slope at this time will be approximately zero, since the velocity  $V$  will be constant for a linear displacement. This transition point between non-linear and linear displacement was identified as the point of global failure by van Asch et al. (2007) in an analysis of the Super-Sauze mudslide. Similar behaviour is found for slopes analysed in our model, as will be discussed in the results section. This allows for simple detection of the critical point being when  $\Delta V / \Delta t$  becomes sufficiently close to zero. This method works for both stable and failed slopes and is relatively efficient, eliminating the need to store, track and evaluate the linearity of displacement.

Once the critical point has been reached, a decision on whether failure has occurred or the slope has stabilised is required. For stabilised slopes, the average displacement of the slope should be negligible. However, for unstable slopes, the displacement will be much larger as the slope continues to deform. We therefore choose to specify a maximum displacement threshold, above which a slope is considered to have failed. To reduce the scale dependence of this value, it is normalised by the slope height. The maximum displacement threshold for failure is likely to be dependent on local conditions and material properties, and is therefore used as a configurable parameter in the slope detection.

If a failure has occurred on the slope, then the transition to a discrete particle representation for the post-failure landslide is performed. The mass of mobilised material in the landslide is bounded by the failure surface below and at the top by the free surface of the slope. At the start of the landslide phase the volume between these two surfaces is filled with densely packed discrete particles. The particles have a shape and size distribution that gives bulk material properties (void ratio, angle of repose) similar to that of the slope material. The failure plane which defines the lower boundary and the surface on which the DEM particles can slide upon is located along the region with the highest shear, expressed through the equivalent plastic shear strain rate.

### DEM landslide prediction

Once a slope failure is detected and the slip surface has been identified, the post failure stage modelling can commence. Several methods have been developed to predict landslide dynamics, an overview of the most common methods can be found in van Asch et al. (2007). Here we use three dimensional DEM, a meshless numerical method that models collision dominated systems at the particle level. Landslide modelling using DEM in three dimensions has previously been demonstrated by Cleary (2004, 2009) and Cleary and Prakash (2004). In this implementation we represent the particles as non-round super-quadratics. For details of the method used, refer to Cleary (2004).

## RESULTS

A simple slope stability benchmark has been used to validate the SPH model of slope stability analysis. This example will then be used to illustrate the combination of SPH with DEM to simulate a complete slope collapse.

### SPH predictions of slope stability

The geometry consists of an unstable slope as shown in Figure 1 and is taken from (Zienkiewicz et al., 1975). This problem was originally solved in 2D by Zienkiewicz et al. under plane strain conditions. We model the system instead in 3D using 10 m wide transverse slice with periodic boundary conditions. The third dimension cannot be avoided in the analysis of real landslides so needs to be included in the method formulation and testing.

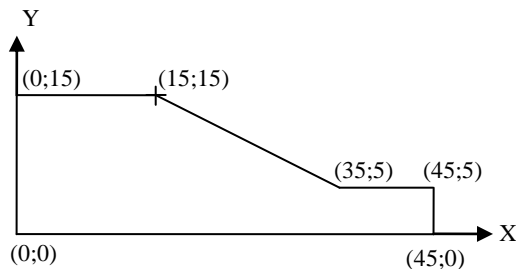


**Figure 1:** Cross-section of the unstable slope with key locations shown (in m).

In the first loading step where gravity was applied, a value of 0.02 for  $\xi$  was found sufficient to damp the undesired oscillations. This value is consistent with that reported in Bui and Fukagawa (2011).

In the second step, the damping term was turned off. The dilatancy coefficient  $\beta$  was assumed equal to the friction coefficient  $\alpha$ . The dilatancy angle has been found to play a relatively minor role on the onset of slope instability (Zienkiewicz et al., 1975) therefore the precise value of this parameter is unimportant in the present simulations. The other material properties used are given in Table 1.

Material properties	E (MPa)	$\nu$	$\phi$ ( $^{\circ}$ )	$\rho$ ( $\text{kg m}^{-3}$ )
Value	200	0.25	20	2038

**Table 1:** Material properties used in the SPH simulations.

Zienkiewicz et al. (1975) determined the critical cohesion below which the slope would become unstable to be about 3 kPa for the configuration of Figure 1. We ran a number of simulations with different values of cohesion (starting from 30 kPa down to 1 kPa) to assess the ability of this model to accurately predict the critical cohesion at failure. In all simulations the particle separation was set to 0.2 m which required about 640,000 particles for the slope discretisation.

Figure 2 displays the average displacement of the slope for cohesion cases ranging from 1 kPa to 30 kPa. The displacement is expressed as a percentage of the slope height (10 m in this case). At time  $t = 1.1$  s, the cohesion was lowered to the physical value ranging from 1 kPa to 30 kPa as explained earlier. This causes the sudden displacement as the slope is no longer in mechanical

equilibrium. For stable configurations the velocity of the slope will rapidly tend back to zero as a new equilibrium is reached. This can be clearly seen in Figure 2 for cohesion values from 4 kPa to 30 kPa. While a small motion was still recorded in these cases, its relative value was sufficiently small to be considered negligible. In contrast, for unstable configurations the displacement keeps increasing, as is observed in Figure 2 for cohesion values ranging from 1 to 3 kPa. From this graph we can infer that the critical cohesion below which the slope becomes unstable is between 3 and 4 kPa, which is in good agreement with the results of (Zienkiewicz et al., 1975).

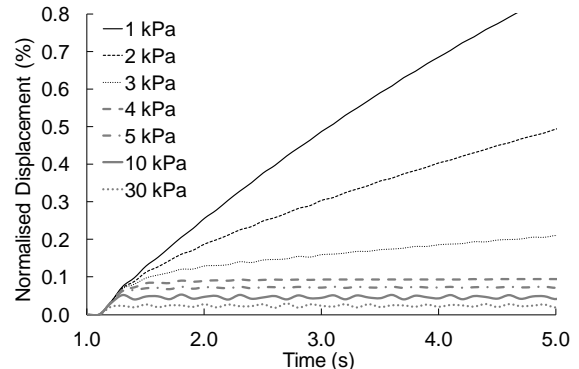


**Figure 2:** Normalised slope displacement for cohesion values from 1 to 3 kPa (unstable, black) and 4 to 30 kPa (stable, grey).

A close-up view of the cross-section of the slope shaded by the von Mises equivalent plastic strain is shown in Figure 3, at  $t = 5$  s (about 4 s after the lowering of the cohesion), for three different values of cohesion corresponding to the three regimes of mechanical response. The post-failure part of the SPH simulations shows the mechanical response of the slope when modelled as an elasto-plastic continuum medium.

- For a cohesion of 30 kPa (Figure 3a), the plastic strain does not exceed 0.4%, with higher plastic strains found at the foot of the slope and close to the boundaries. No failure plane is predicted in this case as the slope is inherently stable.
- For a cohesion of 3 kPa (Figure 3b), a clear region of localised plastic deformation is predicted with a plastic strain within the shear band estimated at about 10%. A region of even higher plastic strain is found at the surface of the slope (the thin red line on the top surface of the slope in Figure 3b), where the plastic strain reaches 20%. Here, the pressure due to gravity is zero and therefore does not play a stabilising role, meaning that points near the surface can readily fail in tension for small values of cohesion. According to the D-P criterion, this material will therefore yield and large plastic strain will be predicted. It would be more accurate to allow for the initiation and development of tensile cracks near the surface since the material will likely fail before it can actually yield. This illustrates ones of the advantages of a discrete (DEM) modelling approach since cracking is naturally supported while continuum modelling of soil ceases to be valid.
- For cohesion of 1 kPa (Figure 3c), the band of localised plastic deformation is wider and much higher values of plastic strain (about 25 %) are predicted

within it. Even larger regions of higher plastic strain (more than 100 %) are predicted near the surface. The shape of the slope at this time is markedly different to that in Figure 3b. The comparatively small value of cohesion causes more material to deform plastically. This is evidenced by the difference in shape between Figure 3b and 3c. In Figure 3b the block above the failure plane retains its original shape while in Figure 3c the upper block has experienced stronger deformation. Again, these observations indicate that a DEM model will be more appropriate for the post-failure analysis because the large amount of failed material will behave more as a collection of interacting discrete entities rather than as a continuum.

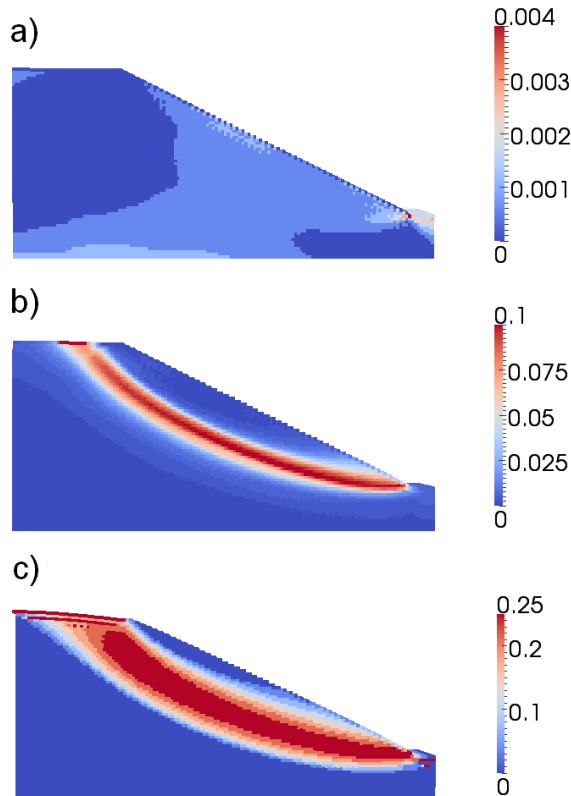


**Figure 3:** SPH predictions of equivalent plastic strain at  $t = 5$  s. a)  $c = 30$  kPa (stable regime), b)  $c = 3$  kPa (critical limit), c)  $c = 1$  kPa (unstable regime). A different scale range has been used in each case to clearly display the strain field contours.

### SPH to DEM transition

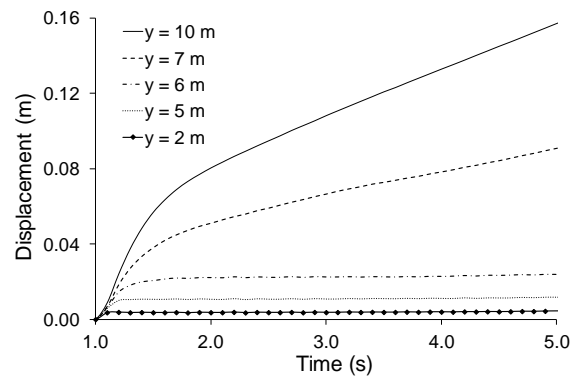


**Figure 4:** Cumulative slope displacement at different heights with  $x = 25$  m for cohesion 3 kPa. After failure, the displacement becomes linear.

Figure 4 shows the slope displacement over time at different heights along the centre of the slope ( $x = 25$  m in Figure 1). The slope studied had cohesion of 3 kPa. The displacement increases with time for the higher points on the slope ( $y = 10$  m and  $y = 7$  m), but remains fairly constant after 1.5 s at points lower than  $y = 6$  m. The displacement is initially non-linear, becoming linear at approximately 2 s. The normalised displacement threshold was specified at 0.1%, based on the onset of instability shown in Figure 3. Using this displacement value, the slope was predicted to have failed at 2 s.

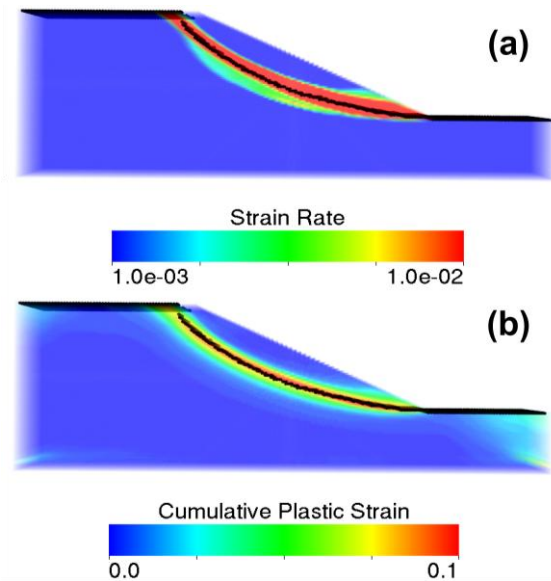


**Figure 5:** (a) Slip surface (black line) and strain rate (in  $s^{-1}$ ) at failure, and (b) slip surface and cumulative plastic strain after 5 s.

After failure, the geometry of the slip surface was calculated, based on the regions of highest shear. Figure 5(a) displays the strain rate and calculated slip surface at the time of failure ( $t = 2$  s) for a slope with a cohesion of 3 kPa. The slip surface lies along the centre of the high strain band and coincides with the highest accumulated plastic strain of the slope after 5 s shown in Figure 5(b). This suggests that an estimate of the slip surface based on the instantaneous strain rate is reliable.

The volume between the slip surface and top surface of the slope was filled with DEM particles with properties

matching the material properties of the slope. The particles had a fairly rounded shape, with a uniform distribution of aspect ratios between 0.7-0.8 and 0.8-0.9, with a major axis length between 0.25 and 0.50 m. In this instance, we assumed the particles were not cohesive, since after failure the sliding mass is essentially non-cohesive.

### DEM simulations of post failure collapse

After transition of the mobilised slope mass to the discrete representation, the resulting DEM particles then move freely under the load applied by the particles above. The flow immediately after the transition is shown in Figure 6a. A small band of particles near the base of the slip plane are moving at approximately 1 m/s. The front of the avalanche is travelling faster at approximately 2 m/s. The particles flow down the slope along the failed slip plane until they come to rest. Figure 6b shows the landslide 4 s after failure. Almost all of the material is moving as a single mass at the same speed (2.5 m/s). The final landslide deposit is shown in Figure 6c. It has stopped with approximately half the material remaining on the failed slip plane and the remainder coming to rest on the horizontal floor.

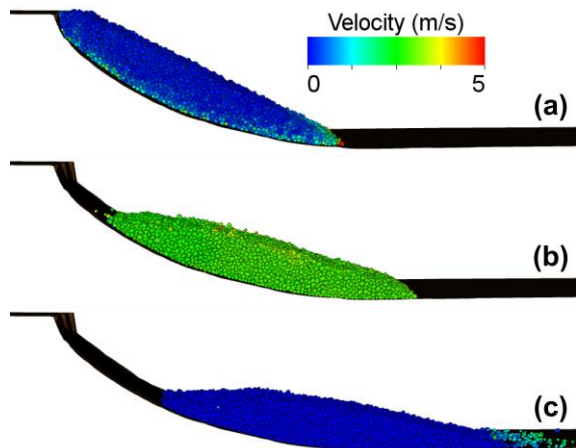


**Figure 6:** DEM prediction of the avalanche at (a) just after failure, (b) 4 s after failure, and (c) at rest, 8 s after failure.

The simplified geometry of this slope means that the avalanche process is not complex, since it lacks topographical features such as gullies and ridgelines which can have a significant effect on the post-failure flow. However the inclusion of such features has been demonstrated by Cleary and Prakash (2004).

### CONCLUSION

A combined SPH-DEM approach has been developed for the simulation of all phases of landslides. A non-associative Drucker-Prager plastic model has been used with SPH to determine the onset of slope failure. The displacement of the slope, the equivalent plastic strain and strain rate are all used as combined indicators to identify failure initiation and the mobilised landslide mass. This is then converted to a discrete form and its subsequent collapse, flow and deposition are predicted using DEM.

The SPH predictions have been compared to available data from the literature and close agreement was found for the estimation of the critical cohesion that leads to the initiation of a landslide. After this initial model validation,

an integrated framework was illustrated by considering the post-failure analysis of the slope using DEM. DEM was able to predict the motion of the material along a solid surface, whose location was defined by the shear plane, and can allow for estimations of run-out distance and final deposit shape of the landslide. This new approach should enable better estimation of risks and potential costs associated to slope failures and landslides.

### REFERENCES

- BUI, H. H., and FUKAGAWA, R., (2011), "An improved SPH method for saturated soils and its application to investigate the mechanisms of embankment failure: Case of hydrostatic pore-water pressure", *Int. J. Numer. Anal. Meth. Geomech.*, 10.1002/nag.1084.
- CLEARY, P. W., (2004), "Large scale industrial DEM modelling", *Eng Computation*, **21**(2-4), 169-204.
- CLEARY, P. W., and PRAKASH, M., (2004), "Discrete-element modelling and smoothed particle hydrodynamics: potential in the environmental sciences", *Philos T R Soc A*, **362**(1822), 2003-2030.
- CLEARY, P. W., (2009), "Industrial particle flow modelling using discrete element method", *Eng Computation*, **26**(6), 698-743.
- CLEARY, P. W., (2010), "Elastoplastic deformation during projectile-wall collision", *Appl Math Model*, **34**(2), 266-283.
- DAS, R., and CLEARY, P. W., (2010), "Effect of rock shapes on brittle fracture using Smoothed Particle Hydrodynamics", *Theor Appl Fract Mec*, **53**(1), 47-60.
- DE SOUZA NETO, E. A., PERIĆ, D., and OWEN, D. R. J. (2008). *Computational Methods for Plasticity*: John Wiley & Sons, Ltd.
- HUNGR, O., and MCDUGALL, S., (2009), "Two numerical models for landslide dynamic analysis", *Comp & Geosci* **35**(5), 978-992.
- MONAGHAN, J. J., (1992), "Smoothed Particle Hydrodynamics", *Annu Rev Astron Astr*, **30**, 543-574.
- MONAGHAN, J. J., (2005), "Smoothed particle hydrodynamics", *Rep Prog Phys*, **68**(8), 1703-1759.
- RANDLES, P. W., and LIBERSKY, L. D., (1996), "Smoothed particle hydrodynamics: Some recent improvements and applications", *Comput Method Appl M*, **139**(1-4), 375-408.
- VAN ASCH, T. W. J., MALET, J. P., VAN BEEK, L. P. H., and AMITRANO, D., (2007), "Techniques, issues and advances in numerical modelling of landslide hazard", *Bull Soc Geol Fr*, **178**(2), 65-88.
- VAN WESTEN, C. J., VAN ASCH, T. W. J., and SOETERS, R., (2006), "Landslide hazard and risk zonation - why is it still so difficult?", *B Eng Geol Environ*, **65**(2), 167-184.
- ZIENKIEWICZ, O. C., HUMPHESON, C., and LEWIS, R. W., (1975), "Associated and Non-Associated Visco-Plasticity and Plasticity in Soil Mechanics", *Geotechnique*, **25**(4), 671-689.